

# Water Resources Research

## RESEARCH ARTICLE

10.1029/2018WR024633

### Key Points:

- A new surface wetness index was developed from satellite-observed vapor pressure deficit, soil moisture, and surface water cover
- The index is consistent with traditional drought monitors but allows for analyzing the relative importance of water cycle components
- The satellite-based multicomponent index allows for independent monitoring of global drought conditions

### Supporting Information:

- Supporting Information S1

### Correspondence to:

J. Du,  
jinyang.du@ntsg.umt.edu

### Citation:

Du, J., Kimball, J. S., Velicogna, I., Zhao, M., Jones, L. A., Watts, J. D., et al. (2019). Multicomponent satellite assessment of drought severity in the Contiguous United States from 2002 to 2017 using AMSR-E and AMSR2. *Water Resources Research*, 55. <https://doi.org/10.1029/2018WR024633>

Received 27 DEC 2018

Accepted 23 MAY 2019

Accepted article online 6 JUN 2019

## Multicomponent Satellite Assessment of Drought Severity in the Contiguous United States From 2002 to 2017 Using AMSR-E and AMSR2

J. Du<sup>1</sup> , J. S. Kimball<sup>1</sup> , I. Velicogna<sup>2,3</sup>, M. Zhao<sup>2</sup> , L. A. Jones<sup>1</sup>, J. D. Watts<sup>4</sup>, Y. Kim<sup>1</sup>, and G. A<sup>2</sup>

<sup>1</sup>Numerical Terradynamic Simulation Group, W.A. Franke College of Forestry and Conservation, The University of Montana, Missoula, MT, USA, <sup>2</sup>Department of Earth System Science, University of California, Irvine, Irvine, CA, USA,

<sup>3</sup>Jet Propulsion Laboratory, California Institute of Technology, Pasadena, CA, USA, <sup>4</sup>Woods Hole Research Center, Falmouth, MA, USA

**Abstract** The Advanced Microwave Scanning Radiometer for the Earth Observing System and Advanced Microwave Scanning Radiometer 2 sensors (AMSR) have provided multifrequency microwave measurements of the global terrestrial water cycle since 2002. A new AMSR surface wetness index (ASWI) was developed by analyzing the near-surface atmospheric vapor pressure deficit (VPD), surface volumetric soil moisture (VSM), and land surface fractional open water (FW) time series from an established AMSR Land Parameter Data Record (LPDR). The ASWI allows for multicomponent and independent satellite assessments of near-surface drought conditions by exploiting the weighted anomalies of VPD, VSM, and FW. Comparisons between ASWI and more traditional drought metrics, including the Palmer moisture anomaly index (PDSI-Z) and the U.S. Drought Monitor, showed generally consistent classifications of drought severity for three major droughts over the Contiguous United States since 2002. The ASWI showed moderate ( $0.3 \leq R \leq 0.7$  for 56% of area) to strong ( $R > 0.7$  for 29% of area) correlations with the PDSI-Z during the summer months (June–August) from 2002 to 2017. ASWI and PDSI-Z differences were attributed to AMSR retrieval uncertainties and the different aspects of drought represented by the indices. Comparisons between ASWI and the Gravity Recovery and Climate Experiment drought severity index (GRACE-DSI) showed strong correspondence ( $R = 0.61$ ) in regions where possible long-term total water storage changes occurred. The sole reliance of the ASWI on satellite microwave remote sensing and continuing AMSR2 operations enables effective global monitoring of drought conditions while providing new information on the atmosphere, soil, and surface water components of drought.

**Plain Language Summary** Extreme hydrologic events affect the economy, environment, and society. The anomalies of the water cycle components are associated with drought events. Considering the capability of multifrequency microwave remote sensing in observing multiple water cycle components, this study developed a new surface wetness index by analyzing near-surface atmospheric vapor pressure deficit, volumetric soil moisture, and land surface water inundation time series from an established satellite data record. The new index showed consistent assessment of major drought events relative to traditional drought monitors while providing enhanced information on the water cycle components of drought. A combined analysis of the index with satellite total water storage measurements provides complementary information on the different aspects of droughts, including relatively dynamic surface water changes and slower evolving groundwater conditions. The index enables independent and continuous satellite assessment of global drought conditions.

## 1. Introduction

The contiguous United States (CONUS) has experienced severe droughts since 2002, which have caused profound impacts to the environment and economy (Gerken et al., 2018; Griffin & Anchukaitis, 2014; Hoerling et al., 2014; Pielke et al., 2005). Drought is a natural disaster associated with the prolonged shortage of water stored in the lower atmosphere or near surface soil and groundwater (Wilhite & Glantz, 1985). Persistent continental drought is often associated with sea surface temperature anomalies (AghaKouchak et al., 2015; Dai, 2011), while regional flash drought, characterized by a rapid rate of intensification (Otkin et al., 2018) and generally driven by anomalously warm temperatures and low precipitation (Mo & Lettenmaier, 2016), may be exacerbated by local land-atmosphere interactions (Gerken et al., 2018). Climate variability

can have cascading impacts on the terrestrial water cycle at local to regional scales, leading to meteorological drought exemplified by a shortage of precipitation or increase of potential evapotranspiration, agricultural drought characterized by below-normal soil moisture, or relatively slower-progressing hydrological drought associated with declining terrestrial water storage (AghaKouchak et al., 2015; Dai, 2011; Dracup et al., 1980; Heim, 2002).

Quantifying the dynamics of the major water cycle components and their climatological mean values is crucial to detecting and monitoring drought, and clarifying the associated driving factors and consequences. Aside from in situ point measurements and hydrological model simulations of key water cycle variables (Dai et al., 2004; Palmer, 1965; Wood et al., 2015), remotely sensed drought indicators, including satellite precipitation and soil moisture observations, and satellite-based drought indices, have greatly advanced capabilities for low-cost and large-scale drought assessment (AghaKouchak et al., 2015). For example, satellite precipitation data were used for operational monitoring of global meteorological drought (AghaKouchak & Nakhjiri, 2012), while Mu et al. (2013) used a 12-year record of MODIS (Moderate Resolution Imaging Spectroradiometer) observations to construct a Drought Severity Index (DSI) incorporating vegetation greenness and evapotranspiration (ET) anomalies for drought assessment. The DSI derived from optical-infrared remote sensing enables near real-time drought monitoring, but its applicability is constrained by noise effects from atmospheric aerosols, clouds, or insufficient solar illumination (Mu et al., 2013).

Progress in microwave remote sensing of global soil moisture over the past two decades has improved the capacity for satellite monitoring of agricultural drought. In particular, soil moisture products derived from AMSR-E (Advanced Microwave Scanning Radiometer for the Earth Observing System) and other spaceborne microwave sensors have been applied for operational drought assessment and crop growth monitoring (Bolten et al., 2010; Yin et al., 2018). Recent satellites designed for global soil moisture monitoring include the European Space Agency SMOS (Soil Moisture Ocean Salinity) and National Aeronautics and Space Administration SMAP (Soil Moisture Active Passive) missions, which provide lower frequency (L-band) microwave observations that have shown promising results in tracking agricultural drought (Martínez-Fernández et al., 2016; Sadri et al., 2018). For hydrological drought, satellite gravimetric measurements of total water storage (TWS) changes from GRACE (Gravity Recovery And Climate Experiment) and the associated drought indices developed from these data have been successful in evaluating persistent drought and pluvial events (Thomas et al., 2014; Geruo et al., 2017; Zhao et al., 2017a, 2017b).

Other studies have adopted a more comprehensive approach to drought monitoring extending beyond single-type drought assessments. This approach incorporates a multivariate and systematic view of drought representing multiple water cycle components that are physically connected through the terrestrial water balance, and where the different types of drought are interconnected (AghaKouchak et al., 2015; Hao & Singh, 2015; Xia et al., 2014). By empirically or statistically combining multiple drought indices or hydrological variables, the multivariate approaches have been successfully applied to drought monitoring and forecast systems (Hao & AghaKouchak, 2013; Hao & AghaKouchak, 2014; Yan et al., 2017).

Global warming is expected to promote greater frequency and intensity of drought (Trenberth et al., 2014). Despite significant advancements in drought research, it is still challenging to achieve timely detection and consistent monitoring of the onset and progression of drought, particularly under rapidly developing flash drought conditions or in regions with sparse or inconsistent in situ monitoring networks. Similar constraints characterized the start of the historic 2012 Great Plains Drought (Yan et al., 2018) and 2017 North Plains Drought (Otkin et al., 2018) that recently impacted major portions of the contiguous United States (CONUS).

The AMSR satellite record includes AMSR-E and the follow-on AMSR2 sensors, which provide multifrequency passive microwave brightness temperature retrievals that are sensitive to surface moisture. The AMSR record also provides consistent global coverage, moderate spatial resolution and 1- to 3-day repeat observations that are relatively insensitive to potential noise effects from variable solar illumination, clouds, and atmosphere aerosol contamination. These attributes enable regional drought assessments derived solely from satellite observations (Du et al., 2017; Sadri et al., 2018), along with potentially enhanced understanding of the complex hydrologic and climatic processes that occur during drought events (Mishra & Singh, 2010; Swain et al., 2014; Trenberth et al., 2014). The effective use of global satellite observations can also greatly enhance drought monitoring capabilities by incorporating near-real time, large-scale measurements of multiple contributing hydrological variables (Heim, 2002). In particular, consistent long-term satellite

observations of surface soil moisture and air humidity (Yin et al., 2018; Du, Kimball, Reichle et al., 2018) have strong potential utility for early drought detection (AghaKouchak et al., 2015; Otkin et al., 2018). The quantification of drought impacts on surface and ground water storage is also essential for effective water resource management (Castle et al., 2014). The potential for multiaspect drought assessment is enabled by the variable sensitivity of different AMSR microwave frequencies to different water cycle components (Du et al., 2017).

In this study, we developed a new satellite-based surface wetness index using AMSR multifrequency passive microwave remote sensing of key water cycle elements for detecting drought events. The AMSR Surface Wetness Index (ASWI) is derived as a multivariate index incorporating daily satellite retrievals of near surface atmospheric vapor pressure deficit (VPD), surface volumetric soil moisture (VSM) and fractional surface water inundation (FW) from an established AMSR Land Parameter Data Record (LPDR; Jones et al., 2010; Du et al., 2017). The ASWI relies solely on satellite retrievals and is intended to provide independent and comprehensive assessments of land surface wetness, incorporating the weighted information of atmospheric moisture demand, near-surface soil moisture, and surface water inundation dynamics.

The ASWI is potentially applicable for assessing both drought and pluvial conditions. In this study, we applied the ASWI record to evaluate recent major drought events occurring within the CONUS domain and available satellite record (2002–2017). The ASWI results were compared with more traditional metrics representing different aspects of drought, including the Palmer moisture anomaly index (PDSI-Z), U.S. Drought Monitor (USDM), and GRACE Drought Severity Index (GRACE-DSI). The following sections contain a detailed description of the methods (section 2), results (section 3), discussion (section 4), and conclusions (section 5) from this study.

## 2. Methods

### 2.1. Study Domain

The study was carried out for the CONUS domain and three selected subregions representing diverse climate, land cover, and hydrological conditions (Figure 1). Land cover variability within the CONUS domain was represented by the MODIS (MCD12C1) IGBP (International Geosphere-Biosphere Programme) land cover classification (Friedl et al., 2002). Vegetation cover generally decreases from east-to-west across the domain, following the regional moisture gradient, and with different regional resilience to climate change (Melillo et al., 2014). A relatively humid climate dominates regions east of the 100th meridian, whereas semiarid to arid climate conditions are more common in the western CONUS (Thompson et al., 2004). In the arid west, groundwater replenishment is heavily dependent on precipitation and snowmelt infiltration contributes significantly to groundwater recharge in mountainous areas (Melillo et al., 2014).

The CONUS subregions selected for this study include the Great Plains, the state of California and the North-Central climatological division of Minnesota (Figure 1). The Great Plains are characterized by a semiarid climate with annual rainfall generally less than 30 inches (Melillo et al., 2014). Most of the Great Plains are susceptible to drought due to an imbalance between water supply from rainfall and relatively high water loss from ET (Melillo et al., 2014); local ecosystems in the Plains region mainly consist of managed cropland, natural grassland and shrubland (Taylor et al., 2015). California, like much of the western CONUS, has experienced severe drought in recent years, which has impacted both natural and managed ecosystems. The California Central Valley, in particular, is characterized by a semiarid climate and extensive croplands (Figure 1) that are intensively managed and irrigated, while much of the region has a well-developed infrastructure for water capture and storage in managed reservoirs and groundwater wells for municipal and agricultural water use (Tanaka et al., 2006). Three major documented drought events occurred over the Great Plains and California subregions within the recent (2002–2017) satellite record and are highlighted in this study (section 3.1). We also performed additional analyses for the north-central climatological division of Minnesota (Figure 1), which is one of the 344 climate divisions defined by the National Climatic Data Center for representing nearly homogenous climatic regions (Keim et al., 2003; Quiring & Ganesh, 2010). The selected division is part of the state of Minnesota, which is characterized by a humid continental climate and the presence of over 15,000 lakes greater than 4 ha in area (Winter, 1977).

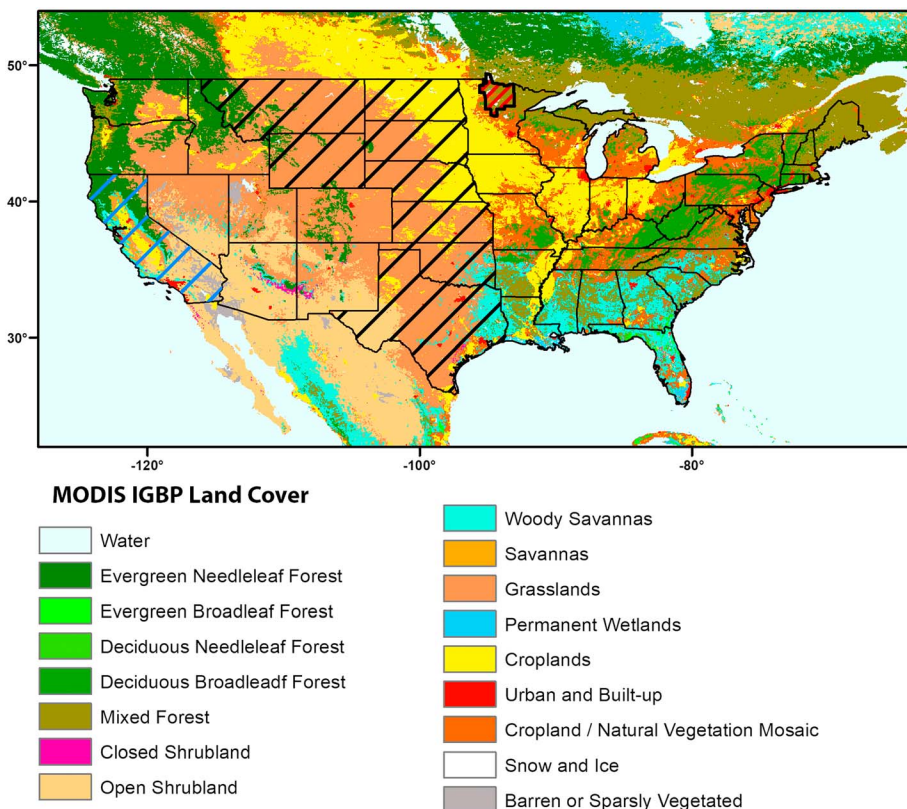


**Figure 1.** Contiguous U.S. domain with U.S. state boundaries delineated and the three subregions highlighted in this study, including the Great Plains (black hash line), California (blue hash line), and north-central climatological division of Minnesota (red hash line). Land cover conditions are represented by the Moderate Resolution Imaging Spectroradiometer (MODIS) International Geosphere-Biosphere Programme (IGBP) global land cover map.

## 2.2. Algorithm Development

### 2.2.1. AMSR Sensors and LPDR

Spaceborne microwave sensors such as AMSR-E (De Jeu et al., 2008; Jackson et al., 2010; Kawanishi et al., 2003; Njoku et al., 2003), AMSR-2 (Imaoka et al., 2012), SMOS (Kerr et al., 2010), and SMAP (Chan et al., 2016; Entekhabi et al., 2010) utilize microwave frequencies that are sensitive to key hydrological variables of the global water cycle, including atmospheric water vapor, soil moisture, and surface water inundation. Among these instruments, AMSR-E (2002–2011) and its successor AMSR2 (2012–present) were designed for monitoring key water cycle components and have provided global twice daily (1:30 and 13:30) and multi-frequency (C- to W-band) brightness temperature ( $T_b$ ) measurements for more than 15 years. The spatial and temporal resolutions of AMSR global observations are about 25 km and 1–3 days, respectively (Kawanishi et al., 2003). The strong sensitivity of AMSR observations to land surface wetness and relatively favorable spatial and temporal coverage over the CONUS domain have promoted the use of AMSR-derived land surface products for regional drought assessment (Geruo et al., 2017; Yin et al., 2019). Lower frequency (L-band) satellite microwave sensors, such as SMAP and SMOS, have coarser sensor footprints than AMSR but similar temporal fidelity, and with potentially enhanced sensitivity to soil moisture that may provide additional synergistic information for drought detection gained through overlapping multifrequency satellite microwave observations (Du, Kimball, Galantowicz et al., 2018; Sadri et al., 2018).

The AMSR LPDR provides a global daily record of key terrestrial environmental parameters at 25-km resolution, including FW, atmosphere precipitable water vapor (PWV), daily maximum/minimum surface air temperature ( $T_{mx}/T_{mn}$ ), vegetation optical depth, and VSM (Du et al., 2017). The LPDR algorithm estimates multiple land surface parameters by decomposing the multifrequency microwave emission signals from the different AMSR channels and polarizations into individual contributions from atmosphere and land features

**Table 1**  
*Regression Coefficients (Slope Only) and Coefficient of Determination ( $R^2$ ) for Calibrating AMSR2 Morning Retrievals Against Those of AMSR-E*

IGBP Land Cover Type	Slope for VPD/ VSM/FW	$R^2$ for VPD/ VSM/FW
Evergreen needleleaf forest	0.89/0.99/1.00	0.95/0.93/0.98
Evergreen broadleaf forest	0.67/0.94/1.00	0.82/0.92/0.98
Deciduous needleleaf forest	0.89/0.94/0.95	0.90/0.88/0.96
Deciduous broadleaf forest	0.85/0.97/1.00	0.91/0.85/0.97
Mixed forests	0.88/0.97/1.00	0.93/0.92/0.98
Closed shrublands	0.92/0.99/0.99	0.97/0.96/0.98
Open shrublands	0.98/0.98/0.96	0.99/0.98/0.97
Woody savannas	0.90/0.95/0.97	0.95/0.94/0.98
Savannas	0.96/0.96/0.95	0.96/0.06/0.97
Grasslands	0.98/0.98/0.96	0.99/0.96/0.97
Permanent wetlands	0.95/1.00/0.96	0.89/0.96/0.98
Croplands	0.98/0.96/0.98	0.93/0.87/0.98
Urban and built-up	0.88/0.89/0.97	0.44/0.41/0.94
Cropland/natural vegetation mosaic	0.85/0.98/1.00	0.86/0.85/0.97
Barren or sparsely vegetated	0.98/1.00/0.97	0.99/0.99/0.98

Note. IGBP = International Geosphere-Biosphere Programme; VPD = vapor pressure deficit; VSM = volumetric soil moisture; FW = fractional open water.

based on an iterative inversion framework and radiative transfer theory (Du et al., 2016, 2017; Jones et al., 2010).

To ensure consistency between AMSR-E and AMSR2 portions of the LPDR, the AMSR2  $T_b$  observations were harmonized with the AMSR-E record using a Double Difference calibration approach (Du et al., 2014). Quantitative global LPDR assessments show favorable retrieval performance for FW ( $R \geq 0.75$ ; root-mean-square error, RMSE  $\leq 0.059$ ), PWV ( $R = 0.92$ ; RMSE  $\leq 4.66$  mm),  $T_{\text{mx}}/T_{\text{mn}}$  ( $R \geq 0.89$ ; RMSE  $\leq 3.46$  °C), and VSM ( $0.630 \leq R \leq 0.835$ ;  $0.031 \text{ cm}^3/\text{cm}^3 \leq \text{RMSE} \leq 0.059 \text{ cm}^3/\text{cm}^3$ ; Du et al., 2017). The LPDR was recently extended to include microwave retrievals of near-surface VPD derived from AMSR PWV and surface air temperature retrievals using a Clausius-Clapeyron and Magnus formula based approximation (Du et al., 2018). The resulting VPD global record showed favorable agreement with independent station measurements ( $R \geq 0.80$ ;  $0.48 \text{ kPa} \leq \text{RMSE} \leq 0.69 \text{ kPa}$ ) and similar performance to VPD estimates derived from global reanalysis data (Du, Kimball, Reichle, et al., 2018). The LPDR data are posted to a consistent 25-km global Equal-Area Scalable Earth (EASE) Grid projection format (Armstrong & Brodzik, 1995). The current AMSR LPDR (version 2) has been used for a diverse set of science application studies, including quantifying the influence of vegetation and soil moisture conditions on SMAP FW retrievals

(Du, Kimball, Galantowicz, et al., 2018), studying ecosystem water storage and phenology (Brandt et al., 2018; Tian et al., 2018), detecting vegetation isohydry/anisohydry behavior and resilience to drought (Anderegg et al., 2018; Li et al., 2017), and mapping paddy rice planting areas (Song et al., 2018).

The AMSR observations and resulting LPDR retrievals for VPD, VSM, and FW allow for the assessment of water cycle responses to extreme climate events by providing key environmental baseline and anomaly information. In particular, VPD represents the atmospheric moisture demand that drives land surface ET (Running & Nemani, 1988); the AMSR VSM retrieval describes moisture conditions within the top (~1-cm) layer of surface soil, which affects mass and energy exchange between the soil and atmosphere, and is interactive with root-zone soil moisture (Crow & Wood, 2003; Walker & Houser, 2001). The top layer soil moisture observed by AMSR is also highly sensitive to meteorological anomalies and capable of detecting short-term droughts (Yuan et al., 2015). FW is directly linked to the surface water inundation and storage component of the terrestrial water budget (Zou et al., 2018), while VSM and FW collectively define the bulk water supply available to meet atmospheric moisture (VPD) demands affecting ET and latent energy exchange. Together, VPD, VSM, and FW can serve as an integrated land surface wetness indicator for monitoring meteorological, agricultural, and hydrological drought, while the associated AMSR retrievals provide the means for satellite observations of global drought events under nearly all-weather conditions.

Despite the intersensor calibration of the AMSR  $T_b$  record, remaining residual differences between the AMSR2 and AMSR-E portions of the LPDR can contribute uncertainty to temporal trends and climatology conditions derived from the long-term record (Du et al., 2017). To further enhance LPDR consistency, we assume that the global mean values of a given LPDR parameter temporally averaged over the respective AMSR-E and AMSR2 periods are the same within a given IGBP global land cover class. The AMSR2 LPDR morning data were then empirically adjusted to the AMSR-E record using land parameter specific linear regression models established for different land cover classes assuming a zero intercept (Table 1). The AMSR2 and AMSR-E retrievals are highly correlated for most land cover classes, except for urban and built-up areas representing ~0.49% of the global land area, which is not expected to affect overall ASWI performance. The resulting adjustment reduces systematic bias between the AMSR-E and AMSR2 portions of record while preserving LPDR variability due to environmental changes.

Considering the overall higher accuracy of LPDR morning retrievals (Du et al., 2017), the newly calibrated LPDR VPD, VSM, and FW morning estimates were used to construct the ASWI monthly record over the CONUS domain and 15-year study period (August 2002 to August 2017). A major gap in the AMSR satellite record occurs between the end of AMSR-E operations in October 2011 and the beginning of AMSR2

operations in May 2012. In addition, the ASWI record is only derived for nonfrozen conditions when valid LPDR retrievals can be made (Du et al., 2017).

### 2.2.2. ASWI Construction

The ASWI is defined as the weighted average of three components, VPD-Z, VSM-Z, and FW-Z, which are the standardized anomalies or  $Z$  scores (henceforth denoted by the letter  $Z$ ) of the VPD, VSM, and FW parameters (denoted by the letter  $P$ ) calculated on a monthly and grid cell basis from the bias-adjusted LPDR global daily record (equation (1)).

$$\begin{aligned} \text{ASWI} &= \sum_{i=1}^3 W_i Z_i \\ Z_i &= \frac{P_i - \bar{P}_i}{\sigma_i} \\ W_i &= \frac{\text{CV}_i}{\sum_{i=1}^3 \text{CV}_i} \end{aligned} \quad (1)$$

where  $\text{CV}_i = \frac{\sigma_i}{\bar{P}_i}$  is the coefficient of variation,  $\sigma_i$  is the temporal standard deviation, and  $\bar{P}_i$  is the climatological mean of monthly  $P_i$  for a given month and grid cell. The  $Z$  value, which is a standardized measurement of the degree of deviation from the climatological mean, is a robust indicator of drought severity (Mu et al., 2013; Zhao et al., 2017a, 2017b). The VPD-Z value was multiplied by  $-1$  in this study to be consistent with the other  $Z$  components, so that the positive (negative) sign corresponds to wet (dry) conditions.

The weighted combination of  $Z$  values for VPD, VSM, and FW was used to construct the ASWI based on their CV values, which enables a multispect assessment of surface wetness less susceptible to artifacts introduced from satellite retrieval uncertainties. A smaller CV suggests the associated parameter is likely less informative in drought assessment due to less variability detected by the AMSR LPDR. However, a smaller CV may also reflect the limited ability of AMSR in mapping land surface parameters under certain conditions, including dense vegetation (Du et al., 2017). For example, the soil emission signal observed by the AMSR sensors decreases exponentially with increasing vegetation cover, leading to relatively small VSM CV values for July over densely forested areas of the eastern United States (Figures 1 and 2b). The relatively high VPD CV in coastal areas is likely due to small climatological mean values especially for the northwest coastal states where similarly high CV values were observed for all four seasons (Seager et al., 2015). We also set zero weight to parameters with a climatological mean smaller than 0.005 due to low reliability of the CV calculated with a small denominator. The units of VPD and VSM are KPa and  $\text{cm}^3/\text{cm}^3$ , respectively, and FW is dimensionless, ranging from 0 (no inundation) to 1 (complete inundation) within a grid cell. Accordingly, no FW CV values were used for constructing the ASWI over arid and semiarid areas with minimal surface water cover (Figure 2c). Grid cells with a climatological mean FW  $> 0.2$  were also excluded in this study due to larger AMSR land parameter retrieval uncertainties in these areas (Du et al., 2017).

### 2.2.3. ASWI Uncertainty Estimation

To quantify the ASWI uncertainties, reference ASWI data sets were constructed using the above approach (section 2.2.2), but with the daily VSM, FW, and VPD retrievals perturbed by random noise. For simplicity, the noise levels ( $\pm 0.48$  KPa for VPD,  $\pm 0.057$  for FW, and  $\pm 0.042 \text{ cm}^3/\text{cm}^3$  for VSM) were defined from the AMSR-E data record, which has similar accuracy to AMSR2 (Du et al., 2017, Du, Kimball, Reichle, et al., 2018). Differences between the observed and reference ASWI values were then used to evaluate ASWI performance. Mean absolute error (MAE) values were also calculated from the monthly ASWI records and reference values to characterize uncertainty.

## 2.3. Ancillary Data Sets for Evaluating ASWI

The ASWI results were evaluated against three other more traditional moisture and drought related metrics, including (a) the monthly Palmer moisture anomaly index (PDSI-Z) obtained from the operational climate monitoring system of the National Oceanic and Atmospheric Administration's National Centers for Environmental Information (<https://www.ncdc.noaa.gov/climate-monitoring/>; Palmer, 1965; Karl, 1986; Heim, 2002), (b) USDM ranked drought severity data distributed by the National Drought Mitigation Center (<http://droughtmonitor.unl.edu>; Svoboda et al., 2002; Lawrimore et al., 2002), and (c) the GRACE measurement based global drought severity index (GRACE-DSI; Tapley et al., 2017; Watkins et al., 2015;

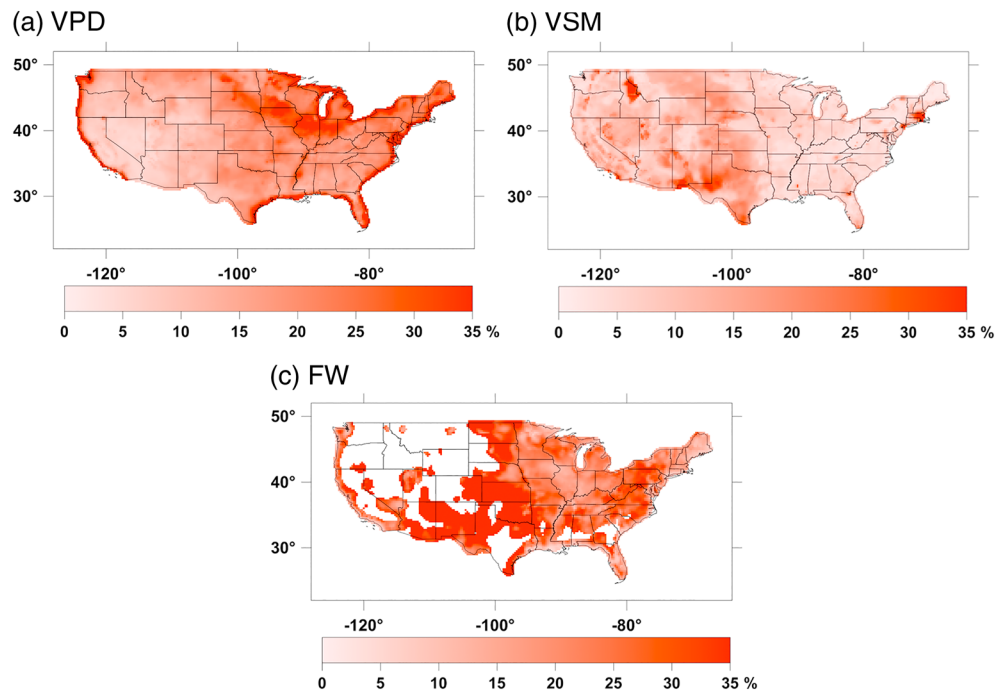


**Figure 2.** Example July coefficient of variation values over the contiguous U.S. domain for the three Land Parameter Data Record parameters used to construct the Advanced Microwave Scanning Radiometer surface wetness index (ASWI), including vapor pressure deficit (VPD; a), volumetric soil moisture (VSM; b), and fractional open water (FW; c) for the 2002–2017 study period. The coefficient of variation values serve as weights of the ASWI components, enabling multispectra assessment of drought conditions while reducing the effects of satellite retrieval uncertainties.

Wiese et al., 2016; Zhao et al., 2017a, 2017b). A detailed summary of these indices is provided in the supporting information section of this paper.

#### 2.4. ASWI Evaluation

Qualitative comparisons were made between the ASWI record and the other drought indices for three major drought events occurring within the CONUS domain during the 2002–2017 study period. These

severe droughts included (a) the 2012 Great Plains Drought (Hoerling et al., 2014), (b) the 2012–2015 California Drought (Griffin & Anchukaitis, 2014), and (c) the 2017 Northern Plains Drought (Gerken et al., 2018). The respective PDSI-Z, USDM, and ASWI data from August 2012, June 2014, and August 2017 were used for plotting relative drought severity maps and assessing the associated events from each index. To be comparable with the USDM, which adopts a five-category drought classification scheme, the PDSI-Z and ASWI data were similarly grouped into five drought severity classes, five wet classes and 1 normal condition class (Table 2). The classifications are associated with the historical occurrence of drought or wet conditions. Considering different time lengths of the data sets used for calculating USDM, ASWI, and PDSI-Z, the data ranges of PDSI-Z and ASWI wetness categories are determined empirically in two steps. First, an equal interval method was used to partition the respective negative and positive index distributions into five dry and five wet classes. An additional “Normal Condition” class was then derived by merging respective wetter and drier portions of the “Abnormally Dry” and “Abnormally Wet” class distributions.

**Table 2**  
Surface Wetness Classifications and Corresponding Values of USDM, PDSI-Z and ASWI

Surface wetness class	Data range		
	USDM	PDSI-Z	ASWI
Exceptional drought	4	-4.0 or less	-2.0 or less
Extreme drought	3	-3.0 to -3.99	-1.5 to -1.99
Severe drought	2	-2.0 to -2.99	-1.0 to -1.49
Moderate drought	1	-1.0 to -1.99	-0.5 to -0.99
Abnormally dry	0	-0.5 to -0.99	-0.25 to -0.49
Normal condition	N/A	-0.49 to 0.49	-0.24 to 0.24
Abnormally wet	N/A	0.5 to 0.99	0.25 to 0.49
Moderately wet	N/A	1.0 to 1.99	0.5 to 0.99
Severely wet	N/A	2.0 to 2.99	1.0 to 1.49
Extremely wet	N/A	3.0 to 3.99	1.5 to 1.99
Exceptionally wet	N/A	4.0 or greater	2.0 or greater

Note. USDM = U.S. Drought Monitor; ASWI = Advanced Microwave Scanning Radiometer surface wetness index; PDSI-Z = Palmer moisture anomaly index; N/A = not applicable.

Respective AMSR VSM, FW, and VPD Z component influences to the bulk ASWI assessment were illustrated using a red-green-blue (RGB) map with color intensity calculated by equation (2).

$$CI_i = \frac{Z_i}{Z_1 + Z_2 + Z_3} \cdot 255 \quad (2)$$

The Z component value in equation (2) was set to zero if it had a different sign than the bulk ASWI value, indicating no positive contribution from the component to the overall drought assessment. The CI level shows the relative importance of a single ASWI component in evaluating overall drought conditions.

Quantitative evaluations of the ASWI data were conducted by calculating their temporal correlations with the corresponding PDSI-Z record over the CONUS domain. Since no AMSR LPDR retrievals were made under frozen conditions, the comparisons were limited to the northern hemisphere summer months (June–August) from 2002 to 2017. In addition, the ASWI data were temporally smoothed using a moving average method and varying window sizes from 1 to 12 months for comparisons with the GRACE-DSI record. The GRACE-DSI represents the integrated drought impacts on TWS (Long et al., 2013), which includes deeper groundwater storage changes that likely evolve slower than dynamic surface hydrological state variables (Zhao et al., 2017a, 2017b). The resulting ASWI data smoothed using N-month moving average represent average surface wetness conditions for a selected month and the preceding N-1 months of record for each grid cell. The highest temporal correlation coefficients calculated using the GRACE-DSI and smoothed ASWI record were then obtained for the MASCON polygons and posted to the 25-km global EASE Grid projection along with the associated optimum window sizes. The comparisons were performed over the entire CONUS domain, but caution is needed to interpret the results over higher latitudes and altitudes where greater occurrence of snow, ice, and frozen soil conditions can degrade the ASWI time series. Correspondence between the ASWI record and the other drought metrics was primarily determined using Pearson's correlation coefficient ( $R$ ).

### 3. Results

#### 3.1. Drought Severity Maps

##### 3.1.1. The 2012 Great Plains Drought

The 2012 Great Plains Drought was the most severe drought since 1895 in the region based on the cumulative rainfall deficit, and coincided with a strong negative El Niño–Southern Oscillation climate phase (i.e., La Niña; Hoerling et al., 2014; Rippey, 2015). The drought started in May and peaked in August, sweeping the Great Plains and causing about \$12 billion in economic losses (Hoerling et al., 2014). The USDM, PDSI-Z, and ASWI drought severity maps all showed widespread drought across the CONUS domain, with exceptional drought conditions in the Central Great Plains region (Figures 3a–3c) during August 2012. In the ASWI RGB component influence map (Figure 3d), the drought-plagued regions show similar contributions from VPD-Z, FW-Z, and VSM-Z to the overall ASWI drought level.

Different from the USDM (Figure 3a), which shows severe to exceptional drought in southern Nevada and northern Georgia, the PDSI-Z (Figure 3b) and ASWI (Figure 3c) show similar above-normal wet conditions for these areas. The ASWI classification mainly reflects wetter surface soil moisture conditions and greater FW inundation extent in these areas indicated from the AMSR observations (Figure 3d). Severe to exceptional drought conditions were classified by both the USDM (Figure 3a) and ASWI (Figure 3c) over the upper and central portions of the Mississippi basin, where the ASWI assessment is mainly influenced by below-normal FW-Z cover in the region (Figure 3d); these results contrast with the PDSI-Z pattern in this region (Figure 3b), which indicates relatively less drought severity to above-normal wet conditions (e.g., eastern Illinois).

##### 3.1.2. The 2012–2015 California Drought

The 2012–2015 California Drought was the worst drought of the last millennium for the region, with profound impacts on local hydrological and ecological environments (Asner et al., 2016; Griffin & Anchukaitis, 2014; Thomas et al., 2017). The drought caused about \$2.7 billion in annual economic losses in 2015 alone (Howitt et al., 2015). Anomalous dry conditions were documented across the southwest CONUS in June 2014 by the USDM (Figure 4a), PDSI-Z (Figure 4b), and ASWI metrics (Figure 4c). The California Central Valley was among the regions most affected by the drought, represented by severe to

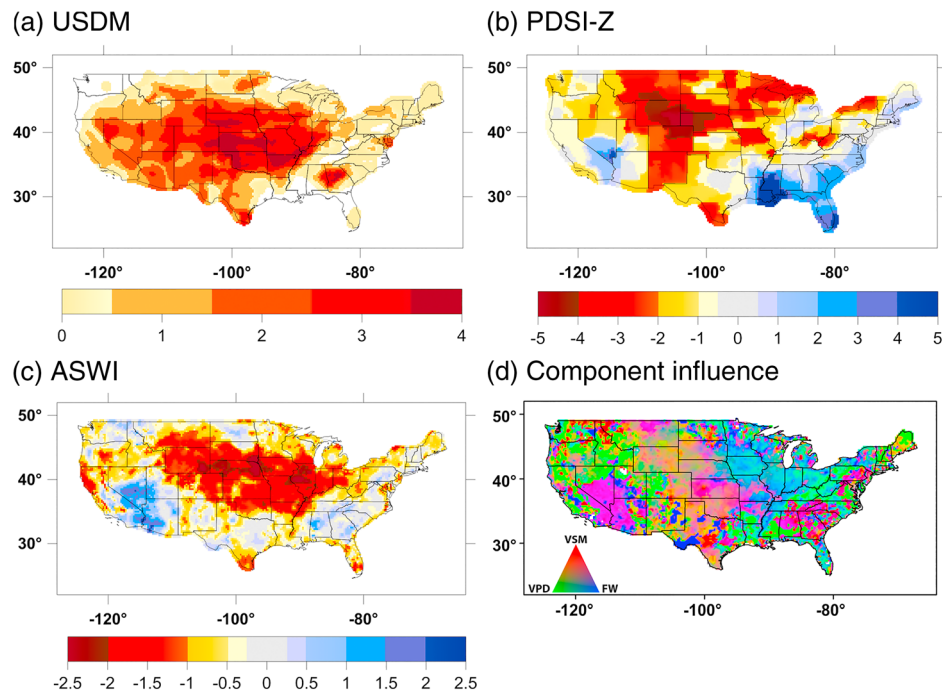


**Figure 3.** Drought severity maps for August 2012 highlighting the 2012 Great Plains Drought. Drought metrics represented include U.S. Drought Monitor (USDM; a), Palmer moisture anomaly index (PDSI-Z; b), and Advanced Microwave Scanning Radiometer surface wetness index (ASWI; c); the ASWI red-green-blue (RGB) component influence map is also presented (d) showing the relative importance of vapor pressure deficit (VPD), volumetric soil moisture (VSM), and fractional open water (FW) to the aggregate ASWI assessment. The color schemes in Figures 3a–3c are consistent in representing the surface wetness classifications detailed in Table 2.

exceptional drought levels from all three indices. The Central Valley area also shows similar contributions from excessive VPD and below-normal VSM and FW levels to the overall ASWI drought signal (Figure 4d).

While the ASWI results are generally consistent with the other indices in capturing the California drought, larger differences among the indices occur over northern Texas, western Oklahoma, and Kansas for the same period. In these regions, the USDM (Figure 4a) predominantly shows varying degrees of drought while the PDSI-Z (Figure 4b) and ASWI (Figure 4c) metrics show wetter-than-normal conditions. The ASWI classification in these areas mainly stems from above-normal near-surface soil moisture observed by AMSR (Figure 4d). Overall, the ASWI shows a drought distribution pattern consistent with the USDM and PDSI metrics for this period, but with greater spatial detail and generally milder drought classifications.

### 3.1.3. The 2017 Northern Plains Drought

The 2017 Northern Plains Drought was a severe flash drought that rapidly developed from late May to September 2017 and was associated with anomalously low convective precipitation (Gerken et al., 2018). The drought sparked widespread wildfires and caused approximately \$2.6 billion in losses to the agricultural sector alone (Hoell et al., 2019). The epicenter of the drought was in Montana where the central and eastern portions of the state are classified as severe to exceptional drought conditions by all three indices (Figure 5). For the state of Washington, Oregon, and northern Idaho, the USDM (Figure 5a) and ASWI (Figure 5c) show less drought severity than the PDSI-Z (Figure 5b). In Montana, the ASWI drought signal is primarily due to exceptionally low soil moisture conditions, though VPD, VSM, and FW show similar contributions in the most severely affected epicenter areas (Figure 5d). For the other northwestern states, the ASWI drought pattern is primarily due to excessive atmospheric water demand (Figure 5d).

In contrast to the widespread drought conditions of the region in August, comparatively little drought was reported by the USDM in May 2017 (Figure 6a). However, anomalous low precipitation and high temperatures were observed for the month (Wang et al., 2019), while both the PDSI-Z and ASWI (Figures 6b and 6c) detected severe spring drought onset in eastern Montana and North Dakota, which preceded and exacerbated more severe summer drought conditions across the region (Gerken et al., 2018; Otkin et al., 2018).

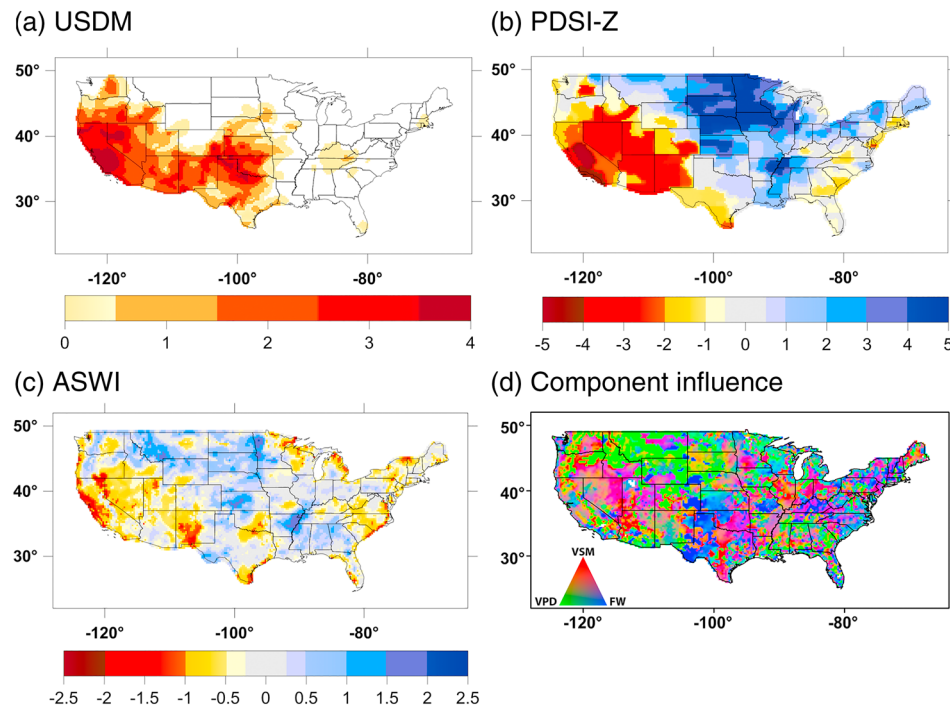


**Figure 4.** Drought severity maps for June 2014 highlighting the 2012–2015 California Drought. Drought metrics represented include U.S. Drought Monitor (USDM; a), Palmer moisture anomaly index (PDSI-Z; b), and Advanced Microwave Scanning Radiometer surface wetness index (ASWI; c); the red-green-blue (RGB) component influence map (d) shows the relative importance of vapor pressure deficit (VPD), volumetric soil moisture (VSM), and fractional open water (FW) to the aggregate ASWI assessment. The color schemes in Figures 4a–4c are consistent in representing the surface wetness classifications detailed in Table 2.

The ASWI component influence map also indicated that the major contributions to the drought initially stemmed from anomalously high VPD levels (Figure 6d), which intensified surface evaporation and soil moisture depletion (Gerken et al., 2018; Otkin et al., 2018).

Additional case studies involving a 2007 drought event (Luo & Wood, 2007) and relatively mild drought conditions in May 2010 (Yan et al., 2018) are included in the Supplementary section of the paper. ASWI, PDSI, and USDM time series over the state of Oklahoma are also included in the supporting information, highlighting a region where drought frequently occurs and the ASWI retrievals are less affected by data gaps from frozen soil or snow conditions.

### 3.2. Quantitative Analysis

#### 3.2.1. Comparisons Between ASWI and PDSI-Z

The PDSI-Z and ASWI data were overall moderately correlated ( $R = 0.54$ ) for the CONUS domain and 2002–2017 summer months (June–August; Figure 7). Approximately 29%, 56%, and 15% of the CONUS domain showed strong ( $R > 0.7$ ), moderate ( $0.3 \leq R \leq 0.7$ ), and weak ( $R < 0.3$ ) correlations between the ASWI and PDSI-Z records, respectively. About 85.8% of the CONUS grid cells were significantly correlated at a 95% confidence level. The ASWI showed generally stronger correspondence with the PDSI-Z than its component variables VPD-Z ( $R = 0.50$ ), VSM-Z (0.48), and FW-Z (0.39). The ASWI generally showed stronger correlations with PDSI-Z over more arid and less vegetated areas (e.g., CONUS central and western regions) relative to eastern and northwestern CONUS regions characterized by a more humid temperate climate and extensive forest cover (Figure 1). Overall, CONUS croplands and grasslands were among the areas showing the best ASWI and PDSI-Z agreement. Much weaker ASWI and PDSI-Z correlations ( $R < 0.3$ ) occurred in lake-abundant areas surrounding the Great Lakes, especially over northern Minnesota (Figure 7). The North Central climatological division of Minnesota (Figure 1) showed no meaningful correspondence between the ASWI and PDSI-Z metrics ( $R = 0.06$ ), which may reflect the different hydrological variables represented in each metric.

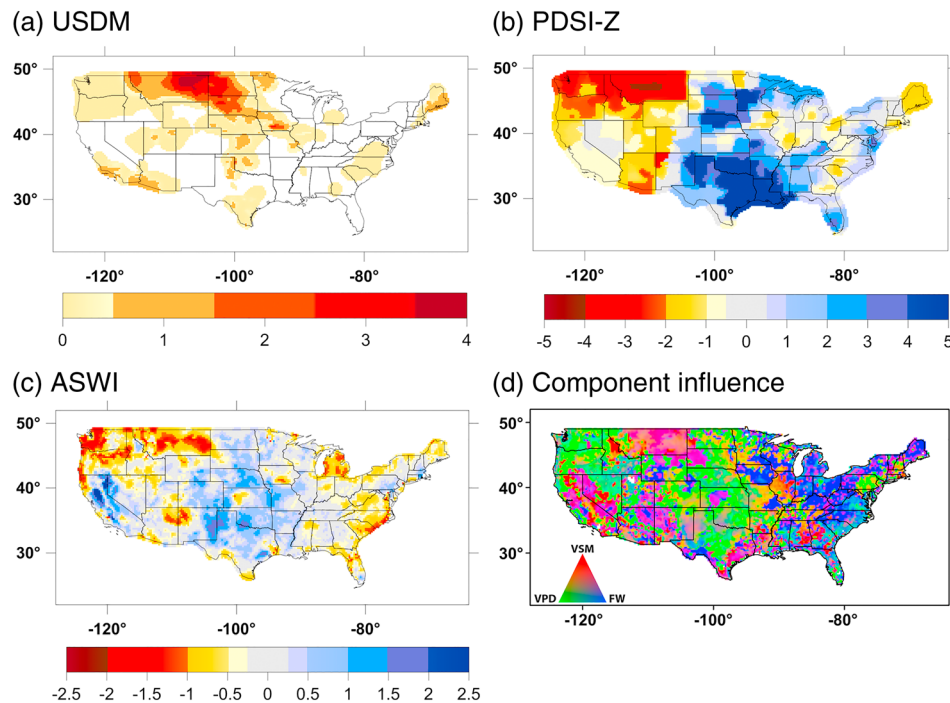


**Figure 5.** Drought severity maps for August 2017 representing the 2017 Northern Plains Drought; drought metrics represented include U.S. Drought Monitor (USDM; a), Palmer moisture anomaly index (PDSI-Z; b), and Advanced Microwave Scanning Radiometer surface wetness index (ASWI; c); the red-green-blue (RGB) map (d) shows the relative importance of vapor pressure deficit (VPD), volumetric soil moisture (VSM), and fractional open water (FW) to the aggregate ASWI assessment. The color schemes in Figures 5a–5c are consistent in representing the surface wetness classifications detailed in Table 2.

### 3.2.2. Comparisons Between ASWI and GRACE-DSI

The maximum correlations between the GRACE-DSI monthly record and the ASWI N-month moving average were calculated on the MASCON polygons over the period from August 2002 to July 2017. The overall ASWI correlations with GRACE-DSI were moderate ( $R = 0.35$ ) over the CONUS domain (Figure 8). About 77.2% of the domain showed statistically significant correlations ( $p < 0.05$ ). The lower latitudes generally showed stronger ASWI and GRACE-DSI correspondence than the higher latitudes, which was attributed to a generally longer non-frozen season and fewer gaps in the data record at lower latitudes. The ASWI and GRACE-DSI correlations were much higher than the domain-average where the ASWI optimum moving window size was  $\geq 8$  months ( $R = 0.61$ ). Among these regions are the California Central Valley and High Plains, which experienced rapid groundwater depletion from irrigation water withdrawals (Scanlon et al., 2012) and severe droughts during the study period (section 3.1); the High Plains region also covers much of the Great Plains, extending across eight states from South Dakota to Texas. In contrast, other areas including the Great Lakes region showed much lower ASWI and GRACE-DSI correspondence, similar to the correlation pattern observed between ASWI and the other drought metrics (e.g., Figure 7).

Further ASWI performance assessments were made over California and the north-central climatological division of Minnesota (Figure 1) using GRACE-DSI monthly data and ASWI (a) monthly and (b) 12-month moving averaged data. For the California region, the ASWI monthly data were moderately correlated with the GRACE-DSI record ( $R = 0.44$ ), while the correlations increased to 0.74 using the ASWI 12-month moving average record (Figure 9a). For Minnesota, the monthly ASWI data were moderately correlated with the GRACE-DSI record ( $R = 0.38$ ), while the correlation increased to 0.65 after the ASWI 12-month moving average was applied (Figure 9b). The stronger GRACE-DSI correspondence with the temporally aggregated ASWI record in this region may reflect temporal lag effects between ASWI surface water conditions and slower evolving groundwater changes detected from GRACE. However, the monthly GRACE record is generally too coarse to resolve finer scale heterogeneity in these relationships.

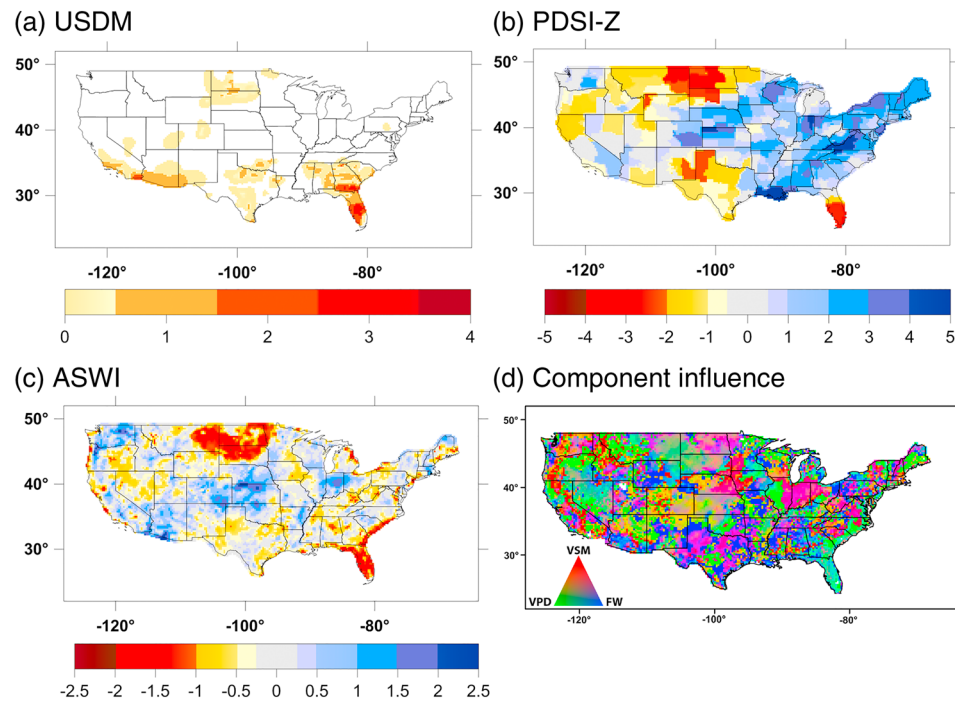


**Figure 6.** Drought severity maps for May 2017 representing the onset of the 2017 Northern Plains Drought; drought metrics represented include U.S. Drought Monitor (USDM; a), Palmer moisture anomaly index (PDSI-Z; b), and Advanced Microwave Scanning Radiometer surface wetness index (ASWI; c); the red-green-blue (RGB) map (d) shows the relative importance of vapor pressure deficit (VPD), volumetric soil moisture (VSM) and fractional open water (FW) to the aggregate ASWI assessment. The color schemes in Figures 6a–6c are consistent in representing the surface wetness classifications detailed in Table 2.

### 3.2.3. ASWI Uncertainties

The estimated ASWI uncertainties for the major CONUS land cover types are similar in level ( $\sim 0.42$ ) and indicate generally favorable performance over more than 97% of the CONUS domain (Table 3). However, the estimated ASWI uncertainty generally increases in areas with greater vegetation cover. Grasslands, shrublands, and barren or sparsely vegetated lands show the lowest ASWI uncertainties ( $MAE < 0.4$ ) and are mainly distributed in the semiarid central and western CONUS regions (Figure 1). Forest lands characterized by higher vegetation biomass cover show higher ASWI uncertainties, with MAE levels ranging from 0.49 to 0.51; these areas largely occur in CONUS eastern and northwestern forests which have a relatively humid climate. The ASWI uncertainties were estimated based on reported AMSR LPDR error levels over the global domain (Du et al., 2017) and may be larger/smaller for a particular region where higher/lower LPDR errors occur.

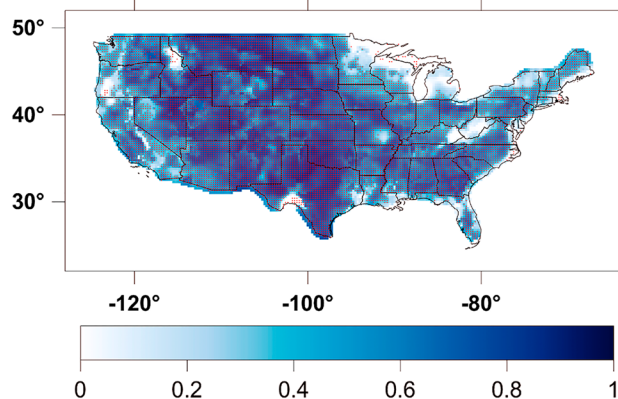


**Figure 7.** ASWI and PDSI-Z correlation ( $R$ ) pattern for the summer months (June–August) from 2002 to 2017 over the CONUS domain. Grid cells with significant correlations ( $p < 0.05$ ) are marked by red dots. ASWI = Advanced Microwave Scanning Radiometer surface wetness index; PDSI-Z = Palmer moisture anomaly index; CONUS = contiguous United States.

## 4. Discussion

This study presents a new satellite surface wetness index derived from AMSR multifrequency microwave measurements representing key water cycle elements, including atmospheric vapor pressure deficit, surface soil moisture, and water inundation. The combined elements of the ASWI metric represent major components of drought events affecting terrestrial ecosystems, including changes in atmospheric moisture demand and surface water supply sources from soil and standing water. The ASWI enables a multispectrally assessment of surface drought conditions with enhanced microwave sensitivity to the target hydrological variables, while providing monthly temporal fidelity and moderate ( $\sim 25\text{-km}$ ) spatial resolution.

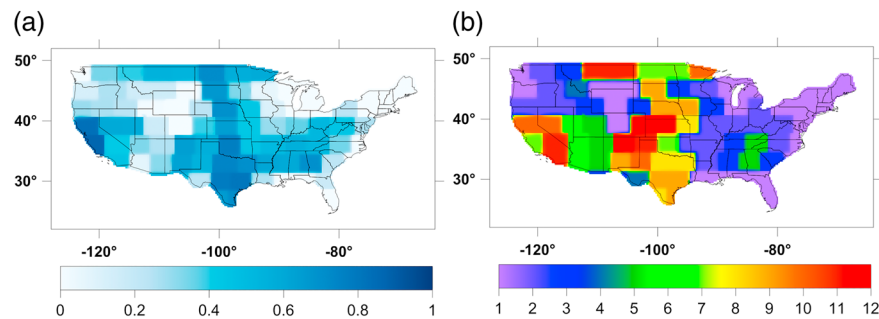


**Figure 8.** Maximum correlations between GRACE-DSI and ASWI (a) time series from August 2002 to July 2016 for the CONUS domain; and the corresponding moving window sizes for ASWI (b). The comparisons were made on MASCON polygons to be spatially consistent between ASWI and GRACE-DSI. GRACE-DSI = Gravity Recovery and Climate Experiment drought severity index; CONUS = contiguous United States; ASWI = Advanced Microwave Scanning Radiometer surface wetness index.

While the ASWI shows overall consistency with more traditional drought indices in characterizing recent major CONUS drought events, some notable differences among the indices were observed that lead to different and even opposite assessment results. For example, the August 2012 drought severity maps show severe drought conditions rated by the USDM in southern Nevada and northern Georgia but classified as wetter-than-normal by the ASWI and PDSI-Z (Figures 3a–3c). Severe to extreme drought conditions were also detected for most of the US Great Plains in an independent study of the 2012 drought event, which used a sophisticated data assimilation framework to combine satellite observations of surface soil moisture with hydrological model simulations (Yan et al., 2018). The reported data assimilation results from Yan et al. (2018) also showed no widespread drought conditions over northern Georgia similar to the ASWI and PDSI results from this study. Contrasting drought assessments from ASWI, PDSI-Z, and the USDM also occurred in other regions such as northern Texas, eastern Oklahoma, and Kansas in June 2014 (Figure 4). The PDSI-Z is sensitive to short-term moisture changes and strongly influenced by input precipitation and air temperature data (Karl, 1986). Transient wetting of surface soils from the same precipitation event dominated the ASWI signal, resulting in general consistency with the PDSI-Z assessment (Figures 3d and 4d) and an independent study using remotely sensed surface soil moisture (Yan et al., 2018).

However, the contrasting USDM severe drought classification for the same region highlighted the accumulated drought impacts on hydrological, ecological, and social environments as interpreted by local experts.

In a separate case, the USDM (Figure 5a) and PSDI-Z (Figure 5b) show divergent drought assessments over Washington, Idaho, and Oregon for August 2017, which may be explained by the ASWI components. As inferred from the ASWI component influence map (Figure 5d), dry air conditions due to warm temperatures and/or low humidity levels were widespread over the Pacific Northwest during this period, while low soil moisture extremes mainly occurred over Montana. As a result, the PDSI-Z likely overemphasized ET related water losses, while the USDM and ASWI showed greater consistency for the region. Similar severe drought conditions were identified along the upper and middle portions of Mississippi river valley by both the USDM (Figure 3a) and ASWI (Figure 3c), which may reflect below-normal surface inundation detected by AMSR (Figure 3d) and decreased runoff considered in the USDM. The contrasting PDSI-Z assessment over eastern Illinois (Figure 3b) may reflect the absence of a surface water component in this metric. Complementary to the USDM and PDSI-Z metrics, the ASWI provides an independent satellite observation based drought assessment with component information on surface moisture conditions that contribute to the interpretation of drought.



**Figure 9.** Comparisons of ASWI 12-month moving averaged data in relation to GRACE-DSI monthly data from August 2002 to July 2016 for the state of California (a) and the north-central climatological division of Minnesota (b). Missing data from October 2011 to May 2012 is due to a gap in the AMSR sensor record. ASWI = Advanced Microwave Scanning Radiometer surface wetness index; GRACE-DSI = Gravity Recovery and Climate Experiment drought severity index; AMSR = Advanced Microwave Scanning Radiometer.

**Table 3**  
*Summary of the ASWI Uncertainties for Major IGBP Land Cover Types in the CONUS Domain*

IGBP land cover type	MAE <sup>a</sup>	Areal proportion <sup>a</sup>
Evergreen needleleaf forest	0.49	6.82%
Deciduous broadleaf forest	0.50	7.72%
Mixed forests	0.51	6.07%
Open shrublands	0.39	13.03%
Woody savannas	0.44	6.34%
Savannas	0.44	1.71%
Grasslands	0.38	24.43%
Croplands	0.40	17.48%
Urban and built-up	0.42	1.34%
Cropland/natural vegetation mosaic	0.44	10.88%
Barren or sparsely vegetated	0.39	1.31%
Overall performance <sup>a</sup>	0.42	97.12%

Note. ASWI = Advanced Microwave Scanning Radiometer surface wetness index; IGBP = International Geosphere-Biosphere Programme; CONUS = contiguous United States.

<sup>a</sup>MAE is the spatial mean absolute error; Areal Proportion is the spatial proportion of the land cover category relative to the larger CONUS land domain. Overall Performance represents the statistics made for all pixels of the listed land cover types.

Timely detection and early warning of rapidly progressing flash droughts is challenging but essential for improving disaster preparedness for stakeholders and government agencies. According to USDM reports, the 2017 Northern Plains Drought intensified from normal to moderate drought conditions in late Spring (Figure 6), to severe to exceptional drought by midsummer (Figure 5), and was purported to be the most severe drought to affect the region in decades (Otkin et al., 2018). However, early drought signals in May 2017 were captured by both PDSI-Z and ASWI and depicted as moderate to severe drought conditions in Montana and the Dakotas (Figures 6b and 6c). Different from the PDSI-Z that relies on station-based meteorological measurements and a water balance model, the ASWI incorporates the direct satellite measurements of hydrologic components. The strong VPD influence in the ASWI drought assessment over Montana and the Dakotas (Figure 6d) further suggests that anomalous high atmospheric water demand intensified soil moisture evaporative losses in May 2017. This analysis is consistent with other studies indicating that a combination of above-normal spring temperatures, strong winds, and low precipitation were responsible for a rapid depletion of soil moisture that exacerbated summer drought in the region (Hoell et al., 2019; Otkin et al., 2018).

Our analysis showed moderate to strong ASWI and PDSI-Z correlations over most of the CONUS domain (section 3.2). The correlations were generally lower in areas with greater vegetation cover, which may reflect greater AMSR retrieval uncertainty in more densely vegetated areas (Table 3). Accordingly, the LPDR VSM and FW retrievals generally have lower CV, larger uncertainties, and greater inconsistency between the two AMSR sensor records (AMSR-E and AMSR-2) over densely vegetated areas (Du et al., 2017). The AMSR VPD retrieval is calculated from saturation vapor pressure and actual vapor pressure estimates, which show strong correspondence with station observations across major global land cover classes (Du, Kimball, Reichle, et al., 2018). The AMSR VPD apparent accuracy is less sensitive to observation time and land cover than the other retrievals, with enhanced performance in areas with larger CV (Du, Kimball, Reichle, et al., 2018). This feature provides for an AMSR monthly VPD-Z metric that is sensitive to both dry and wet anomalies, and with less environmental constraints compared with FW-Z and VSM-Z. Therefore, the CV metric provides a useful indicator of the general quality of the ASWI VPD-Z, VSM-Z, and FW-Z components. Alternatively, Copula function-based approaches are flexible in describing the joint distributions of multiple variables for multivariate drought modeling (Hao & AghaKouchak, 2013; Hao & AghaKouchak, 2014; Yan et al., 2017). However, the uncertainties of the AMSR retrievals vary among the different hydrological variables and land surface conditions. Further studies are needed to statistically combine the satellite retrievals while accounting for potential differences in the underlying parameter uncertainties.

By assigning less weight to ASWI components with smaller CV for a given grid cell, the resulting optimized multiparameter index showed stronger correspondence with the PDSI-Z than the individual ASWI components. In addition to better AMSR performance under low to moderate vegetation cover, the central and southwestern CONUS regions have larger wet/dry dynamic ranges, which may contribute to the stronger correlation between ASWI and PDSI in these areas relative to the more humid temperate eastern forests. Similar to the findings of Yin et al. (2018), the ASWI integrated satellite surface wetness observations are capable of detecting drought over soil moisture-limited regions such as the US Great Plains. However, consistent with the general ASWI and PDSI correlation patterns and the variable AMSR LPDR performance documented from previous studies (Du et al., 2017), our error analysis shows a general increase in ASWI uncertainty from less densely vegetated areas in semiarid climates to more densely forested regions characterized by humid climate conditions. Overall, the ASWI performance is generally favorable over most of the CONUS domain (MAE ~0.42; Table 3).

The ASWI results showed weak correlations with the PDSI-Z around the Great Lakes region, especially across northern Minnesota. The hydrological environment of this region is characterized by abundant

lakes influenced by surface runoff and groundwater conditions, which may be uncoupled from local climate conditions, including temperature and precipitation (Dadaser-Celik & Stefan, 2007; Winter, 1977). Considering the PDSI-Z dependence on meteorological inputs, the ASWI may be a more effective metric of the hydrological water deficit in this region by incorporating AMSR surface soil moisture and water inundation observations.

The overall correlation between the ASWI and GRACE-DSI records was only moderate ( $R = 0.35$ ), which was attributed to the different hydrological variables represented by each index. The GRACE-DSI measures bulk terrestrial water storage changes from multiple factors including soil moisture, surface water inundation, groundwater storage, and snow and ice cover (Abelen et al., 2015; Zhao et al., 2017a, 2017b). Considering the relatively coarse resolution (~300 km) of the GRACE record, these data are most suitable for detecting large-scale TWS changes driven by climate variability and anthropogenic factors (Rodell et al., 2009; Zou et al., 2018). The ASWI, however, is primarily sensitive to near-surface wetness within each 25-km grid cell and is not directly sensitive to groundwater or snow/ice components. Accordingly, the higher latitudes generally showed lower ASWI and GRACE-DSI correlations due to greater data gaps from seasonal frozen conditions and potential snow and ice impacts. The ASWI and GRACE-DSI records may also show inconsistent or even contradictory drought assessments when groundwater variations dominate the TWS signal (e.g., caused by irrigation) and are uncoupled from local weather and seasonal climate impacts on near-surface moisture conditions (Dai, 2011; Rodell et al., 2009). A general time lag between the ASWI and GRACE-DSI response is also apparent (Figure 8b) and may reflect differences between dynamic changes in surface wetness detected from AMSR and slower evolving groundwater changes indicated from GRACE (Zhao et al., 2017a, 2017b).

The ASWI and GRACE-DSI records showed improved correlations ( $R = 0.61$ ) when accounting for temporal lag response differences between the two metrics using optimum moving average window sizes ranging from 8 to 12 months. Most of the regions with optimal moving window size  $\geq 8$  months (Figure 8b) were among the areas having significant changing trends of GRACE TWS from 2002 to 2016 (Zou et al., 2018). These results indicate possible interannual or long-term hydrological changes detected by both GRACE-DSI and ASWI despite their differences in spatial resolution and underlying drivers. For example, a long-term TWS deficit over California detected by GRACE coincides with a persistent multiyear drought induced by climate factors and observed by the AMSR sensors (Figure 9a). The depletion of groundwater in California was also exacerbated by increasing groundwater pumping for irrigation during drought events when surface water availability was lacking (Scanlon et al., 2012). For northern Minnesota, a declining trend in both ASWI and GRACE-DSI records may reflect long-term water budget changes in the larger Great Lakes region, where lake water levels have dropped since the late 1990s (Gronewold & Stow, 2014). These results indicate ASWI utility for assessing both transient wetting and drying events, as well as more persistent hydrological changes.

## 5. Conclusions

The AMSR global satellite record extends from 2002 to present and provides consistent daily observations of near surface atmospheric vapor pressure deficit, soil moisture, and surface water inundation extent. These variables are spatially and temporally dynamic and represent key elements of the terrestrial water cycle, providing new capabilities for satellite monitoring of drought. In this study, we developed a new satellite land surface wetness index based on an established AMSR land parameter record. The ASWI allows for global assessment of terrestrial drought conditions represented by changes in atmospheric water demand, soil moisture, and surface water inundation dynamics. In this study, the ASWI data were found to be consistent with more traditional drought monitors, including the PDSI-Z and USDM, in assessing major drought events over the CONUS domain and 15-year study period (2002–2017). The ASWI also provided additional information on drought severity represented by component changes in atmospheric VPD, soil moisture, and surface water extent. Quantitative comparisons showed overall moderate correlations between ASWI and PDSI-Z monthly data during the summer season ( $R = 0.54$ ). The ASWI and PDSI-Z differences were attributed to one or more factors, including AMSR retrieval uncertainties, differences between satellite measurements and model simulations driven by sparse weather station data, and the different aspects of drought represented by each index. The mean correlation between monthly ASWI and GRACE-DSI records was

relatively low ( $R = 0.35$ ) but showed improved correspondence ( $R = 0.61$ ) for regions where a temporal lag 8 to 12 months was considered between relatively rapid ASWI surface water changes and the slower evolving groundwater signal from GRACE. The ASWI and GRACE-DSI records also showed similar interannual variations and multiyear trends linked with persistent drought and/or climate change over two contrasting CONUS subregions in California and northern Minnesota.

The ASWI is derived solely from AMSR satellite microwave remote sensing, providing global coverage at moderate (25-km) spatial resolution and enhanced microwave sensitivity to near-surface moisture dynamics. While a monthly ASWI record was used in this study, the daily AMSR LPDR enables potential ASWI production with finer temporal fidelity (e.g., daily to weekly). The ASWI also preserves component information on VPD, SM, and FW, which provides for a more comprehensive diagnosis and attribution of drought and pluvial events and impacts on regional ecosystems and water resources. These observations are complementary to more traditional drought indices that rely on ancillary models, sparse weather station observations, or expert assessments. The incorporation of satellite measurements of key hydrologic components in ASWI enables enhanced drought assessment, including timely detection of the rapid onset of flash drought events and observation-based diagnosis of the key factors contributing to drought severity. The combined satellite observations from ASWI and GRACE further allows for multiscale and multitemporal scale assessment of drought, including rapid near-surface moisture variations, less dynamic changes in surface water bodies, and much slower evolving groundwater conditions.

While the ASWI provides for potential global monitoring of mesoscale drought events from the perspective of satellite microwave remote sensing, the AMSR record may be too short to determine an effective climatology for characterizing extreme events. Further sensor intercalibration efforts are expected to improve the precision in quantifying environmental anomalies and trends represented from the AMSR-E and AMSR-2 records. Continuing operations from AMSR2 also enable potential extension of the AWSI record for global monitoring, and new capacity for characterizing and understanding climate variability and water cycle connections.

## Acknowledgments

AMSR-E data are produced by Remote Sensing Systems and sponsored by the NASA Earth Science MEaSUREs DISCOVER Project and the AMSR-E Science Team. Data are available at [www.remss.com](http://www.remss.com). AMSR-E data and land cover classification maps were also provided courtesy of the National Snow and Ice Data Center (NSIDC). The AMSR2 data used for this study were provided courtesy of JAXA. The AMSR LPDR data are publicly available at NSIDC (<https://nsidc.org/data/nsidc-0451>), while the AMSR ASWI record developed from this study is available through NTSG ([http://files.ntsg.umt.edu/data/LPDR\\_v2/Binary/ASWI/](http://files.ntsg.umt.edu/data/LPDR_v2/Binary/ASWI/)). This work was conducted at the University of Montana with funding from the National Aeronautics and Space Administration (NASA; grants NNH15ZDA001N, 80NSSC18K0738, and NNX15AB59G).

## References

- Abelen, S., Seitz, F., Abarca-del-Rio, R., & Güntner, A. (2015). Droughts and floods in the La Plata basin in soil moisture data and GRACE. *Remote Sensing*, 7(6), 7324–7349. <https://doi.org/10.3390/rs70607324>
- AghaKouchak, A., Farahmand, A., Melton, F. S., Teixeira, J., Anderson, M. C., Wardlow, B. D., & Hain, C. R. (2015). Remote sensing of drought: Progress, challenges and opportunities. *Reviews of Geophysics*, 53, 452–480. <https://doi.org/10.1002/2014RG000456>
- AghaKouchak, A., & Nakhjiri, N. (2012). A near real-time satellite-based global drought climate data record. *Environmental Research Letters*, 7(4), 044037. <https://doi.org/10.1088/1748-9326/7/4/044037>
- Anderegg, W. R. L., Konings, A. G., Trugman, A. T., Yu, K., Bowling, D. R., Gabbitas, R., et al. (2018). Hydraulic diversity of forests regulates ecosystem resilience during drought. *Nature*, 561(7724), 538–541. <https://doi.org/10.1038/s41586-018-0539-7>
- Armstrong, R. L., & Brodzik, M. J. (1995). An earth-gridded SSM/I data set for cryospheric studies and global change monitoring. *Advances in Space Research*, 16(10), 155–163. [https://doi.org/10.1016/0273-1177\(95\)00397-W](https://doi.org/10.1016/0273-1177(95)00397-W)
- Asner, G. P., Brodrick, P. G., Anderson, C. B., Vaughn, N., Knapp, D. E., & Martin, R. E. (2016). Progressive forest canopy water loss during the 2012–2015 California drought. *Proceedings of the National Academy of Sciences*, 113(2), E249–E255. <https://doi.org/10.1073/pnas.1523397113>
- Bolten, J. D., Crow, W. T., Zhan, X., Jackson, T. J., & Reynolds, C. A. (2010). Evaluating the utility of remotely sensed soil moisture retrievals for operational agricultural drought monitoring. *IEEE Journal of Selected Topics in Applied Earth Observations and Remote Sensing*, 3(1), 57–66. <https://doi.org/10.1109/JSTARS.2009.2037163>
- Brandt, M., Yue, Y., Wigneron, J. P., Tong, X., Tian, F., Jepsen, M. R., et al. (2018). Satellite-observed major greening and biomass increase in south China karst during recent decade. *Earth's Future*, 6(7), 1017–1028. <https://doi.org/10.1029/2018EF000890>
- Castle, S. L., Thomas, B. F., Reager, J. T., Rodell, M., Swenson, S. C., & Famiglietti, J. S. (2014). Groundwater depletion during drought threatens future water security of the Colorado River Basin. *Geophysical Research Letters*, 41, 5904–5911. <https://doi.org/10.1002/2014GL061055>
- Chan, S. K., Bindlish, R., O'Neill, P. E., Njoku, E., Jackson, T., Colliander, A., et al. (2016). Assessment of the SMAP passive soil moisture product. *IEEE Transactions on Geoscience and Remote Sensing*, 54(8), 4994–5007. <https://doi.org/10.1109/TGRS.2016.2561938>
- Crow, W. T., & Wood, E. F. (2003). The assimilation of remotely sensed soil brightness temperature imagery into a land surface model using ensemble Kalman filtering: A case study based on ESTAR measurements during SGP97. *Advances in Water Resources*, 26(2), 137–149. [https://doi.org/10.1016/S0309-1708\(02\)00088-X](https://doi.org/10.1016/S0309-1708(02)00088-X)
- Dadaser-Celik, F., & Stefan, H. G. (2007). Lake level response to climate in Minnesota. Minneapolis, MN: St. Anthony Falls Laboratory. <http://hdl.handle.net/11299/117628>.
- Dai, A. (2011). Drought under global warming: A review. *Wiley Interdisciplinary Reviews: Climate Change*, 2(1), 45–65.
- Dai, A., Trenberth, K. E., & Qian, T. (2004). A global dataset of Palmer Drought Severity Index for 1870–2002: Relationship with soil moisture and effects of surface warming. *Journal of Hydrometeorology*, 5(6), 1117–1130. <https://doi.org/10.1175/JHM-386.1>
- De Jeu, R. A. M., Wagner, W., Holmes, T. R. H., Dolman, A. J., Van De Giesen, N. C., & Friesen, J. (2008). Global soil moisture patterns observed by space borne microwave radiometers and scatterometers. *Surveys in Geophysics*, 29(4–5), 399–420. <https://doi.org/10.1007/s10712-008-9044-0>

- Dracup, J. A., Lee, K. S., & Paulson, E. G. Jr. (1980). On the definition of droughts. *Water Resources Research*, 16(2), 297–302. <https://doi.org/10.1029/WR016i002p00297>
- Du, J., Kimball, J., Reichle, R., Jones, L., Watts, J., & Kim, Y. (2018). Global satellite retrievals of the near-surface atmospheric vapor pressure deficit from AMSR-E and AMSR2. *Remote Sensing*, 10(8), 1175. <https://doi.org/10.3390/rs10081175>
- Du, J., Kimball, J. S., Galantowicz, J., Kim, S. B., Chan, S. K., Reichle, R., et al. (2018). Assessing global surface water inundation dynamics using combined satellite information from SMAP, AMSR2 and Landsat. *Remote Sensing of Environment*, 213, 1–17. <https://doi.org/10.1016/j.rse.2018.04.054>
- Du, J., Kimball, J. S., & Jones, L. A. (2016). Passive microwave remote sensing of soil moisture based on dynamic vegetation scattering properties for AMSR-E. *IEEE Transactions on Geoscience and Remote Sensing*, 54(1), 597–608. <https://doi.org/10.1109/TGRS.2015.2462758>
- Du, J., Kimball, J. S., Jones, L. A., Kim, Y., Glassy, J., & Watts, J. D. (2017). A global satellite environmental data record derived from AMSR-E and AMSR2 microwave earth observations. *Earth System Science Data*, 9(2), 791. <https://doi.org/10.5194/essd-9-791-2017>
- Du, J., Kimball, J. S., Shi, J., Jones, L. A., Wu, S., Sun, R., & Yang, H. (2014). Inter-calibration of satellite passive microwave land observations from AMSR-E and AMSR2 using overlapping FY3B-MWRI sensor measurements. *Remote Sensing*, 6(9), 8594–8616. <https://doi.org/10.3390/rs6098594>
- Entekhabi, D., Njoku, E. G., O'Neill, P. E., Kellogg, K. H., Crow, W. T., Edelstein, W. N., et al. (2010). The soil moisture active passive (SMAP) mission. *Proceedings of the IEEE*, 98(5), 704–716. <https://doi.org/10.1109/JPROC.2010.2043918>
- Friedl, M. A., McIver, D. K., Hodges, J. C. F., Zhang, X. Y., Muchoney, D., Strahler, A. H., et al. (2002). Global land cover mapping from MODIS: Algorithms and early results. *Remote Sensing of Environment*, 83(1–2), 287–302. [https://doi.org/10.1016/S0034-4257\(02\)00078-0](https://doi.org/10.1016/S0034-4257(02)00078-0)
- Gerken, T., Bromley, G. T., Ruddell, B. L., Williams, S., & Stoy, P. C. (2018). Convective suppression before and during the United States Northern Great Plains flash drought of 2017. *Hydrology and Earth System Sciences*, 22(8), 4155–4163. <https://doi.org/10.5194/hess-22-4155-2018>
- Geruso, A., Velicogna, I., Kimball, J. S., Du, J., Kim, Y., Colliander, A., & Njoku, E. (2017). Satellite-observed changes in vegetation sensitivities to surface soil moisture and total water storage variations since the 2011 Texas drought. *Environmental Research Letters*, 12(1), 17–22. [10.1088/1748-9326/aa6965](https://doi.org/10.1088/1748-9326/aa6965)
- Griffin, D., & Anchukaitis, K. J. (2014). How unusual is the 2012–2014 California drought? *Geophysical Research Letters*, 41, 9017–9023. <https://doi.org/10.1002/2014GL062433>
- Gronewold, A. D., & Stow, C. A. (2014). Water loss from the Great Lakes. *Science*, 343(6175), 1084–1085. <https://doi.org/10.1126/science.1249978>
- Hao, Z., & AghaKouchak, A. (2013). Multivariate standardized drought index: A parametric multi-index model. *Advances in Water Resources*, 57, 12–18. <https://doi.org/10.1016/j.advwatres.2013.03.009>
- Hao, Z., & AghaKouchak, A. (2014). A nonparametric multivariate multi-index drought monitoring framework. *Journal of Hydrometeorology*, 15(1), 89–101. <https://doi.org/10.1175/JHM-D-12-0160.1>
- Hao, Z., & Singh, V. P. (2015). Drought characterization from a multivariate perspective: A review. *Journal of Hydrology*, 527, 668–678. <https://doi.org/10.1016/j.jhydrol.2015.05.031>
- Heim, R. R. Jr. (2002). A review of twentieth-century drought indices used in the United States. *Bulletin of the American Meteorological Society*, 83(8), 1149–1166. <https://doi.org/10.1175/1520-0477-83.8.1149>
- Hoell, A., Perlitz, J., Dewes, C., Wolter, K., Rangwala, I., Quan, X. W., & Eischeid, J. (2019). Anthropogenic contributions to the intensity of the 2017 United States northern Great Plains drought. *Bulletin of the American Meteorological Society*, 100(1), S19–S24. <https://doi.org/10.1175/BAMS-D-18-0127.1>
- Hoerling, M., Eischeid, J., Kumar, A., Leung, R., Mariotti, A., Mo, K., et al. (2014). Causes and predictability of the 2012 Great Plains drought. *Bulletin of the American Meteorological Society*, 95(2), 269–282. <https://doi.org/10.1175/BAMS-D-13-00055.1>
- Howitt, R.; MacEwan, D.; Medellin-Azuara, J.; Lund, J.; Sumner, D. (2015). Economic analysis of the 2015 drought for California agriculture; Center for Watershed Sciences, University of California: Davis, CA, USA.
- Imaoka, K., Maeda, T., Kachi, M., Kasahara, M., Ito, N., & Nakagawa, K. (2012). Status of AMSR2 instrument on GCOM-W1. Proc. SPIE Asia-Pacific Remote Sens., 852815. doi: <https://doi.org/10.1117/12.977774>
- Jackson, T. J., Cosh, M. H., Bindlish, R., Starks, P. J., Bosch, D. D., Seyfried, M., et al. (2010). Validation of advanced microwave scanning radiometer soil moisture products. *IEEE Transactions on Geoscience and Remote Sensing*, 48(12), 4256–4272. <https://doi.org/10.1109/TGRS.2010.2051035>
- Jones, L. A., Ferguson, C. R., Kimball, J. S., Zhang, K., Chan, S. T. K., McDonald, K. C., et al. (2010). Satellite microwave remote sensing of daily land surface air temperature minima and maxima from AMSR-E. *IEEE Journal of Selected Topics in Applied Earth Observations and Remote Sensing*, 3(1), 111–123. <https://doi.org/10.1109/JSTARS.2010.2041530>
- Karl, T. R. (1986). The sensitivity of the Palmer drought severity index and Palmer's Z-index to their calibration coefficients including potential evapotranspiration. *Journal of Climate and Applied Meteorology*, 25(1), 77–86. [https://doi.org/10.1175/1520-0450\(1986\)025<0077:TSOTPD>2.0.CO;2](https://doi.org/10.1175/1520-0450(1986)025<0077:TSOTPD>2.0.CO;2)
- Kawanishi, T., Sezai, T., Ito, Y., Imaoka, K., Takeshima, T., Ishido, Y., et al. (2003). The advanced scanning microwave radiometer for the Earth Observing System (AMSR-E): NASA's contribution to the EOS for global energy and water cycle studies. *IEEE Transactions on Geoscience and Remote Sensing*, 41(2), 184–194. <https://doi.org/10.1109/TGRS.2002.808331>
- Keim, B. D., Wilson, A. M., Wake, C. P., & Huntington, T. G. (2003). Are there spurious temperature trends in the United States Climate Division database? *Geophysical Research Letters*, 30(7), 1404. <https://doi.org/10.1029/2002GL016295>
- Kerr, Y. H., Waldteufel, P., Wigneron, J. P., Delwart, S., Cabot, F., Boutin, J., et al. (2010). The SMOS mission: New tool for monitoring key elements of the global water cycle. *Proceedings of the IEEE*, 98(5), 666–687. <https://doi.org/10.1109/JPROC.2010.2043032>
- Lawrimore, J., Heim, R. R. Jr., Svoboda, M., Swail, V., & Englehart, P. J. (2002). Beginning a new era of drought monitoring across North America. *Bulletin of the American Meteorological Society*, 83(8), 1191–1192. <https://doi.org/10.1175/1520-0477-83.8.1191>
- Li, Y., Guan, K., Gentine, P., Konings, A. G., Meinzer, F. C., Kimball, J. S., et al. (2017). Estimating global ecosystem isohydry/anisohydry using active and passive microwave satellite data. *Journal of Geophysical Research: Biogeosciences*, 122, 3306–3321. <https://doi.org/10.1002/2017JG003958>
- Long, D., Scanlon, B. R., Longuevergne, L., Sun, A. Y., Fernando, D. N., & Save, H. (2013). GRACE satellite monitoring of large depletion in water storage in response to the 2011 drought in Texas. *Geophysical Research Letters*, 40, 3395–3401. <https://doi.org/10.1002/grl.50655>
- Luo, L., & Wood, E. F. (2007). Monitoring and predicting the 2007 US drought. *Geophysical Research Letters*, 34, L22702. <https://doi.org/10.1029/2007GL031673>

- Martínez-Fernández, J., González-Zamora, A., Sánchez, N., Gumuzzio, A., & Herrero-Jiménez, C. M. (2016). Satellite soil moisture for agricultural drought monitoring: Assessment of the SMOS derived Soil Water Deficit Index. *Remote Sensing of Environment*, 177, 277–286. <https://doi.org/10.1016/j.rse.2016.02.064>
- Melillo, J. M., Richmond, T.C., & Yohe, G. W. (Eds.) (2014). Climate change impacts in the United States: The third national climate assessment. 841 pp., Washington, DC: U.S. Global Change Research Program. doi:<https://doi.org/10.7930/J0Z31WJ2>
- Mishra, A. K., & Singh, V. P. (2010). A review of drought concepts. *Journal of Hydrology*, 391(1-2), 202–216. <https://doi.org/10.1016/j.jhydrol.2010.07.012>
- Mo, K. C., & Lettenmaier, D. P. (2016). Precipitation deficit flash droughts over the United States. *Journal of Hydrometeorology*, 17(4), 1169–1184. <https://doi.org/10.1175/JHM-D-15-0158.1>
- Mu, Q. Z., Zhao, M. S., Kimball, J. S., McDowell, N. G., & Running, S. W. (2013). A remotely sensed global terrestrial drought severity index. *Bulletin of the American Meteorological Society*, 94(1), 83–98. <https://doi.org/10.1175/BAMS-D-11-00213.1>
- Njoku, E. G., Jackson, T. J., Lakshmi, V., Chan, T. K., & Nghiem, S. V. (2003). Soil moisture retrieval from AMSR-E. *IEEE transactions on Geoscience and remote sensing*, 41(2), 215–229. <https://doi.org/10.1109/TGRS.2002.808243>
- Otkin, J. A., Svoboda, M., Hunt, E. D., Ford, T. W., Anderson, M. C., Hain, C., & Basara, J. B. (2018). Flash droughts: a review and assessment of the challenges imposed by rapid-onset droughts in the United States. *Bulletin of the American Meteorological Society*, 99(5), 911–919. <https://doi.org/10.1175/BAMS-D-17-0149.1>
- Palmer, W. C. (1965). Meteorological drought, Rep. 45, 58 pp., Washington, D. C.: U.S. Dept. of Commerce (<http://www.ncdc.noaa.gov/oa/climate/research/drought/palmer.pdf>).
- Pielke, R. A. Sr., Doesken, N., Bliss, O., Green, T., Chaffin, C., Salas, J. D., et al. (2005). Drought 2002 in Colorado: An unprecedented drought or a routine drought? *Pure and Applied Geophysics*, 162(8-9), 1455–1479. <https://doi.org/10.1007/s00024-005-2679-6>
- Quiring, S. M., & Ganesh, S. (2010). Evaluating the utility of the Vegetation Condition Index (VCI) for monitoring meteorological drought in Texas. *Agricultural and Forest Meteorology*, 150(3), 330–339. <https://doi.org/10.1016/j.agrformet.2009.11.015>
- Rippey, B. R. (2015). The US drought of 2012. *Weather and Climate Extremes*, 10, 57–64. <https://doi.org/10.1016/j.wace.2015.10.004>
- Rodell, M., Velicogna, I., & Famiglietti, J. S. (2009). Satellite-based estimates of groundwater depletion in India. *Nature*, 460(7258), 999–1002. <https://doi.org/10.1038/nature08238>
- Running, S. W., & Nemani, R. R. (1988). Relating seasonal patterns of the AVHRR vegetation index to simulate photosynthesis and transpiration of forests in different climates. *Remote Sensing of Environment*, 24(2), 347–367. [https://doi.org/10.1016/0034-4257\(88\)90034-X](https://doi.org/10.1016/0034-4257(88)90034-X)
- Sadri, S., Wood, E. F., & Pan, M. (2018). Developing a drought-monitoring index for the contiguous US using SMAP. *Hydrology and Earth System Sciences*, 22(12), 6611–6626. <https://doi.org/10.5194/hess-22-6611-2018>
- Scanlon, B. R., Faunt, C. C., Longuevergne, L., Reedy, R. C., Alley, W. M., McGuire, V. L., & McMahon, P. B. (2012). Groundwater depletion and sustainability of irrigation in the US High Plains and Central Valley. *Proceedings of the National Academy of Sciences*, 109(24), 9320–9325. <https://doi.org/10.1073/pnas.1200311109>
- Seager, R., Hooks, A., Williams, A. P., Cook, B., Nakamura, J., & Henderson, N. (2015). Climatology, variability, and trends in the US vapor pressure deficit, an important fire-related meteorological quantity. *Journal of Applied Meteorology and Climatology*, 54(6), 1121–1141. <https://doi.org/10.1175/JAMC-D-14-0321.1>
- Song, P., Mansaray, L. R., Huang, J., & Huang, W. (2018). Mapping paddy rice agriculture over China using AMSR-E time series data. *ISPRS Journal of Photogrammetry and Remote Sensing*, 144, 469–482. <https://doi.org/10.1016/j.isprsjprs.2018.08.015>
- Svoboda, M., LeComte, D., Hayes, M., Heim, R., Gleason, K., Angel, J., et al. (2002). The drought monitor. *Bulletin of the American Meteorological Society*, 83(8), 1181–1190. <https://doi.org/10.1175/1520-0477-83.8.1181>
- Swain, D. L., Tsiang, M., Haugen, M., Singh, D., Charland, A., Rajaratnam, B., & Diffenbaugh, N. S. (2014). The extraordinary California drought of 2013/2014: Character, context, and the role of climate change. *Bulletin of the American Meteorological Society*, 95(9), S3–S7.
- Tanaka, S. K., Zhu, T., Lund, J. R., Howitt, R. E., Jenkins, M. W., Pulido, M. A., et al. (2006). Climate warming and water management adaptation for California. *Climatic Change*, 76(3-4), 361–387. <https://doi.org/10.1007/s10584-006-9079-5>
- Tapley, B., Flechtner, F., Boening, C., Bettadpur, S., & Watkins, M. (2017). The current status of the grace mission. Paper presented at GRACE Science Team Meeting, Austin, TX.
- Taylor, J. L., Acevedo, W., Auch, R. F., & Drummond, M. A. (2015). Status and trends of land change in the Great Plains of the United States: 1973 to 2000. US Department of the Interior, US Geological Survey.
- Thomas, A. C., Reager, J. T., Famiglietti, J. S., & Rodell, M. (2014). A GRACE-based water storage deficit approach for hydrological drought characterization. *Geophysical Research Letters*, 41, 1537–1545. <https://doi.org/10.1002/2014GL059323>
- Thomas, B. F., Famiglietti, J. S., Landerer, F. W., Wiese, D. N., Molotch, N. P., & Argus, D. F. (2017). GRACE groundwater drought index: Evaluation of California Central Valley groundwater drought. *Remote Sensing of Environment*, 198, 384–392. <https://doi.org/10.1016/j.rse.2017.06.026>
- Thompson, R. S., Shafer, S. L., Anderson, K. H., Strickland, L. E., Pelletier, R. T., Bartlein, P. J., & Kerwin, M. W. (2004). Topographic, bioclimatic, and vegetation characteristics of three ecoregion classification systems in North America: Comparisons along continent-wide transects. *Environmental Management*, 34(S1), S125–S148. <https://doi.org/10.1007/s00267-003-7200-3>
- Tian, F., Wigneron, J. P., Ciais, P., Chave, J., Ogée, J., Peñuelas, J., et al. (2018). Coupling of ecosystem-scale plant water storage and leaf phenology observed by satellite. *Nature ecology & evolution*, 2(9), 1428–1435. <https://doi.org/10.1038/s41559-018-0630-3>
- Trenberth, K. E., Dai, A., Van Der Schrier, G., Jones, P. D., Barichivich, J., Briffa, K. R., & Sheffield, J. (2014). Global warming and changes in drought. *Nature Climate Change*, 4(1), 17–22. <https://doi.org/10.1038/nclimate2067>
- Walker, J. P., & Houser, P. R. (2001). A methodology for initializing soil moisture in a global climate model: Assimilation of near-surface soil moisture observations. *Journal of Geophysical Research*, 106(D11), 11,761–11,774. <https://doi.org/10.1029/2001JD900149>
- Wang, H., Schubert, S. D., Koster, R. D., & Chang, Y. (2019). Attribution of the 2017 northern High Plains drought. *Bulletin of the American Meteorological Society*, 100(1), S25–S29. <https://doi.org/10.1175/BAMS-D-18-0115.1>
- Watkins, M. M., Wiese, D. N., Yuan, D. N., Boening, C., & Landerer, F. W. (2015). Improved methods for observing Earth's time variable mass distribution with GRACE using spherical cap mascons. *Journal of Geophysical Research: Solid Earth*, 120, 2648–2671. <https://doi.org/10.1002/2014JB011547>
- Wiese, D. N., Landerer, F. W., & Watkins, M. M. (2016). Quantifying and reducing leakage errors in the JPL RL05M GRACE mascon solution. *Water Resources Research*, 52, 7490–7502. <https://doi.org/10.1002/2016WR019344>
- Wilhite, D. A., & Glantz, M. H. (1985). Understanding: the Drought Phenomenon: The Role of Definitions. *Water International*, 10(3), 111–120. <https://doi.org/10.1080/02508068508686328>
- Winter, T. C. (1977). Classification of the hydrologic settings of lakes in the north central United States. *Water Resources Research*, 13(4), 753–767. <https://doi.org/10.1029/WR013004p00753>

- Wood, E. F., Schubert, S. D., Wood, A. W., Peters-Lidard, C. D., Mo, K. C., Mariotti, A., & Pulwarty, R. S. (2015). Prospects for advancing drought understanding, monitoring, and prediction. *Journal of Hydrometeorology*, 16(4), 1636–1657. <https://doi.org/10.1175/JHM-D-14-0164.1>
- Xia, Y., Ek, M. B., Mocko, D., Peters-Lidard, C. D., Sheffield, J., Dong, J., & Wood, E. F. (2014). Uncertainties, correlations, and optimal blends of drought indices from the NLDAS multiple land surface model ensemble. *Journal of Hydrometeorol*, 15(4), 1636–1650. <https://doi.org/10.1175/JHM-D-13-058.1>
- Yan, H., Moradkhani, H., & Zarekarizi, M. (2017). A probabilistic drought forecasting framework: A combined dynamical and statistical approach. *Journal of Hydrology*, 548, 291–304. <https://doi.org/10.1016/j.jhydrol.2017.03.004>
- Yan, H., Zarekarizi, M., & Moradkhani, H. (2018). Toward improving drought monitoring using the remotely sensed soil moisture assimilation: A parallel particle filtering framework. *Remote sensing of environment*, 216, 456–471. <https://doi.org/10.1016/j.rse.2018.07.017>
- Yin, J., Zhan, X., Hain, C. R., Liu, J., & Anderson, M. C. (2018). A method for objectively integrating soil moisture satellite observations and model simulations toward a blended drought index. *Water Resources Research*, 54, 6772–6791. <https://doi.org/10.1029/2017WR021959>
- Yin, J., Zhan, X., Liu, J., & Schull, M. (2019). An inter-comparison of Noah model skills with benefits of assimilating SMOPS blended and individual soil moisture retrievals. *Water Resources Research*, 55, 2572–2592. <https://doi.org/10.1029/2018WR024326>
- Yuan, X., Ma, Z., Pan, M., & Shi, C. (2015). Microwave remote sensing of short-term droughts during crop growing seasons. *Geophysical Research Letters*, 42, 4394–4401. <https://doi.org/10.1002/2015GL064125>
- Zhao, M., Geruo, A., Velicogna, I., & Kimball, J. S. (2017a). Satellite observations of regional drought severity in the continental United States using GRACE-based terrestrial water storage changes. *Journal of Climate*, 30(16), 6297–6308. <https://doi.org/10.1175/JCLI-D-16-0458.1>
- Zhao, M., Geruo, A., Velicogna, I., & Kimball, J. S. (2017b). A global gridded dataset of grace drought severity index for 2002–14: Comparison with PDSI and SPEI and a case study of the Australia millennium drought. *Journal of Hydrometeorology*, 18(8), 2117–2129. <https://doi.org/10.1175/JHM-D-16-0182.1>
- Zou, Z., Xiao, X., Dong, J., Qin, Y., Doughty, R. B., Menarguez, M. A., et al. (2018). Divergent trends of open-surface water body area in the contiguous United States from 1984 to 2016. *Proceedings of the National Academy of Sciences*, 115(15), 3810–3815. <https://doi.org/10.1073/pnas.1719275115>